Graphene-enabled low-control quantum gates between static and mobile spins

G. Cordourier-Maruri,[1,2] Y. Omar,[3,4] R. de Coss,[1] and S. Bose[2]

[1]*Departamento de Física Aplicada, Cinvestav-Mérida, A.P. 73 Cordemex, Mérida, Yucatán 97310, México*

[2]*Department of Physics and Astronomy, University College London, Gower Street, London WC1E 6BT, England, United Kingdom*

[3]*Physics of Information Group, Instituto de Telecomunicações, P-1049-001 Lisbon, Portugal*

[4]*CEMAPRE, ISEG, University of Lisbon, P-1200-781 Lisbon, Portugal*

(Received 20 September 2013; revised manuscript received 28 January 2014; published 21 February 2014)

We show that the features of Klein tunneling make graphene a unique interface for implementing low control quantum gates between static and mobile qubits. A ballistic electron spin is considered as the mobile qubit, while the static qubit is the electronic spin of a quantum dot fixed in a graphene nanoribbon. Scattering is the low control mechanism of the gate, which in other systems is very difficult to exploit because of both backscattering and the momentum dependence of transmission. We find that the unique features of Klein tunneling enable quasideterministic quantum gates between the spin of a ballistic electron and a static spin held in a dot, regardless of the momenta or the shape of the incident electron wave function. The Dirac equation is used to describe the system in the one particle approximation, with the interaction between the static and the mobile spins modeled by a Heisenberg Hamiltonian. Furthermore, we discuss an application of this model to generate entanglement between two well-separated static qubits.

DOI: 10.1103/PhysRevB.89.075426 PACS number(s): 03.67.Lx, 73.21.Hb, 85.35.Gv

I. INTRODUCTION

Quantum gates between static and mobile spins can impart scalability to various solid-state quantum information processing (QIP) architectures by effectively enabling gates between distant static qubits. At present, the spin of ballistic electrons is a promising mobile qubit in view of the development of quantum electron optics [1–4]. With such a development, ballistic electron scattering would perhaps be the most effective and the least controlled way to enact a gate between a mobile and a static spin, and it has been suggested recently [5,6] following several schemes for entangling static spins in solid-state structures by scattering [7–12]. Such schemes can be implemented with quantum Hall edge states [1,2], carbon nanotubes [13,14], or a graphene nanoribbon, as we will show here.

While scattering is a unitary process in the combined Hilbert space of the spin and spatial degrees of freedom, it is generically *not* so when solely the spin degree of freedom is considered. However, a quantum gate between two spins is a unitary operation solely in the spin space. Thus, employing scattering for a quantum gate is very tricky and proposed solutions require postselection [5] or resonant conditions valid only for monochromatic electrons [6]. Here we show how graphene nanoribbons, already proposed to host static spin qubits [15,16], can help to overcome all the above problems.

Graphene is a monolayer of carbon atoms packed into a hexagonal crystal structure [17]. It has extraordinary electronic properties [17–19] and presents a high spin coherence time [16]. The last is due to the low spin-orbit coupling in carbon-based materials and because natural carbon consists predominantly of zero-spin isotope ^{12}C, for which the hyperfine interaction is absent [15,20]. Additionally, wrinkles in graphene can be reduced by growing on an appropriate substrate [21], so that spin-orbit interactions are minimal. All this makes graphene a very interesting option to implement spintronic systems.

Electronic transport in graphene is governed by the Dirac-like Hamiltonian [17,18], with electrons behaving as massless Dirac fermions. The relativistic analogy extends to the electron wave function, which is a two-component vector discriminating between the contribution of the two sublattices present in graphene. This degree of freedom is known as *pseudospin* and its states have a defined chirality: the pseudospin is parallel (antiparallel) to the electron (hole) momentum [18]. If the pseudospin is conserved, and a graphene electron is scattered by a potential barrier in one direction, a hole state moving in the opposite direction is created inside the potential, to preserve the pseudospin direction. This allows a perfect electronic transmission through a potential barrier by means of a hole state, analogous to a relativistic phenomena known as Klein tunneling [15,18,22,23]. Additionally, graphene nanoribbons with semiconducting armchair boundaries have a gap between conduction and valence bands [22,24,25] due to transverse confinement, which can be used to localize electrons in a region through electric gating [15].

In this paper we show the conditions required to implement a scattering based two-qubit gate, and we show how this gate can be implemented on a graphene nanoribbon. An application of this model to generate entanglement between two distant quantum dots using a ballistic electron as a mediator is also discussed.

II. GENERAL SETUP

We consider a graphene nanoribbon of width W and with semiconducting armchair boundaries in the y axis. The transverse confinement produces a quantization of the transverse wave vector k_y [15,24]:

$$k_{ny} = \left(n \pm \frac{1}{3}\right)\frac{\pi}{W}, \quad n \in \mathbb{Z}. \tag{1}$$

The band gap is $E_{\text{gap}} = 2\hbar v_F k_{0y}$, with v_F the graphene Fermi velocity ($v_F \approx 10^6$ m s^{-1} [22]), which can be used to make a one-electron quantum dot (QD) with a square potential well [15]. Suppose that the QD has rectangular shape, with

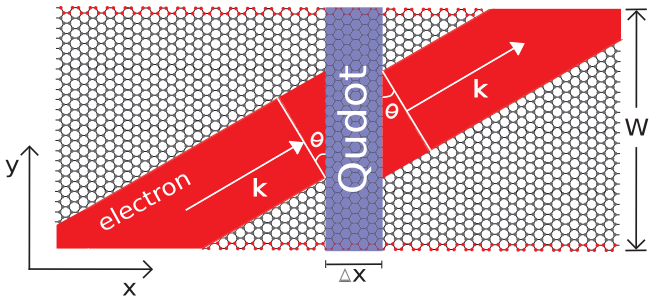

FIG. 1. (Color online) Schematic diagram of an electron elastic scattering with an incident angle θ, on a rectangular QD of Δx length.

the same width as the graphene nanoribbon and with a length Δx. Then, a ballistic electron moving along on the graphene nanoribbon is scattered by the QD, with incident angle θ and energy ϵ_b, as shown in Fig. 1. The transverse confinement is a constraint to the incident angle θ, as the quantization of k_y limits the accessible wave vectors with a fixed energy ϵ_b as

$$\theta = \tan^{-1}\left[\frac{k_{ny}}{\sqrt{\epsilon_b^2/\hbar^2 v_F^2 - k_{ny}^2}}\right]. \tag{2}$$

Thus, frontal scattering ($\theta \approx 0$) is asymptotically obtained when $\epsilon_b \gg \hbar v_F k_{ny}$. This is a constraint in the use of Klein tunnelling in semiconducting armchair graphene nanoribbons, as the total transmission is only present in frontal scattering [22]. Nevertheless, in the following we will show how variations in θ produce only small changes in transmission.

Working in a regime where there is always one static and one ballistic electron, we will approximate the system by a one particle Dirac-like Hamiltonian:

$$\hat{H} = -i\hbar v_F \sigma \cdot \nabla + J\hat{\mathbf{S}}_e \cdot \hat{\mathbf{S}}_i \delta(x), \tag{3}$$

where $\sigma = \{\sigma_x, \sigma_y\}$ are the Pauli matrices for the ballistic electron spin and $\hat{\mathrm{S}}_e$ and $\hat{\mathrm{S}}_i$ are the electronic and impurity spin operators, respectively (the QD is located at $x = 0$). Note that here we have assumed that the scattering process is elastic, so that the wave vectors of the incoming and the outgoing electron are the same. This is indeed well within the parameter scale of our problem, as theoretical studies have estimated the inelastic length and time scales for hot ballistic electrons in graphene to be 100 nm and 0.1 ps, respectively [26]. The elasticity also guarantees that the configuration of *one electron confined to the dot and one electron moving* remains fixed even after the scattering, if $\epsilon_b - \epsilon_{\mathrm{qd}} < E_{\mathrm{gap}}$, where ϵ_{qd} is the QD energy. Thus, treating the QD spin in a manner similar to an Anderson impurity, an effective Heisenberg term has been written in Eq. (3) to reduce the two electron problem to a one electron problem. The Heisenberg interaction is taken to be of delta function form in space with coupling $J \approx 4\Delta x T^2/U$ where

$$T = \epsilon_b \int \psi_b(\boldsymbol{r})\psi_d(\boldsymbol{r})d\boldsymbol{r} \tag{4}$$

and

$$U = \frac{e^2}{4\pi\epsilon_0}\iint \frac{|\psi_d(\boldsymbol{r}_1)|^2|\psi_b(\boldsymbol{r}_2)|^2}{|\boldsymbol{r}_1 - \boldsymbol{r}_2| + \delta} d\boldsymbol{r}_1 d\boldsymbol{r}_2, \tag{5}$$

in which $\delta = 0.0814$ nm is the radial extent of a π orbital in graphene [27] and ψ_b and ψ_d are the ballistic electron and QD wave functions, respectively. Thus, the parameters w, Δx, and ϵ_b can be controlled to reach a desired J value. In principle, the ballistic electron Fermi wavelength $\lambda_F \gg \Delta x$ makes the delta potential a good approximation, but it is still valid for small incidence angles and wider Δx, as we will discuss in the next section. The advantage of the delta potential approximation is that it efficiently reduces the complexity of the problem in a region where resonant behaviors of the wave function are not predominant.

The eigenstates of the Hamiltonian Eq. (3) must include the pseudospin, electron, and QD spin contributions. We consider the QD as a static 1/2-spin particle, with the wave function

$$\psi_{sd} = A\chi_{1/2} + B\chi_{-1/2} = A\begin{pmatrix}1\\0\end{pmatrix} + B\begin{pmatrix}0\\1\end{pmatrix}, \tag{6}$$

in terms of the Pauli vectors $\chi_{\pm 1/2}$. The ballistic electron wave function is modeled as a two-dimensional monochromatic wave moving with a wave vector $k = \epsilon_b/\hbar v_F$ with $k^2 = k_x^2 + k_y^2$. Then, the ballistic electron wave function in the region $x < 0$ is a four-component vector:

$$\psi_b = \begin{pmatrix}1\\ se^{i\theta}\end{pmatrix} \otimes (a\chi_{1/2} + b\chi_{-1/2})e^{i(k_x x + k_y y)} + \begin{pmatrix}1\\ -se^{-i\theta}\end{pmatrix} \otimes (c\chi_{1/2} + d\chi_{-1/2})re^{i(-k_x x + k_y y)}. \tag{7}$$

The first term in the right side of Eq. (7) represents the incident electron, while the second term describes the reflected electron with a probability amplitude r. The transmitted electron wave function has the form

$$\psi_b = \begin{pmatrix}1\\ se^{i\theta}\end{pmatrix} \otimes (f\chi_{1/2} + g\chi_{-1/2})te^{i(k_x x + k_y y)}, \tag{8}$$

for $x > 0$ with a transmission probability amplitude t. Here, $s = \mathrm{sgn}(\epsilon_b)$ generalizes the wave function for the case of a hole. The incident angle $\theta = \tan^{-1}(k_y/k_x)$ depicts the pseudospin direction. In the one particle approximation the entire system wave function can be written as $\Psi = \psi_b \otimes \psi_{sd}$. The proposed wave function contains 12 probability amplitudes to find with boundary and initial conditions. To obtain the boundary conditions, we act similarly to the well-known nonrelativistic delta barrier problem and we have to integrate the Hamiltonian Eq. (3) on an infinitesimally small interval around $x = 0$ as

$$\lim_{\Delta x \to 0}\int_{-\Delta x}^{\Delta x} \hat{H}\Psi(x,y)dx = \lim_{\Delta x \to 0}\int_{-\Delta x}^{\Delta x} \epsilon_b \Psi(x,y)dx. \tag{9}$$

A special problem for this limit evaluation is that in a Dirac-like Hamiltonian the inclusion of a delta potential produces a discontinuity in the wave function. To solve the problem, we allow the components of $\Psi(x,y)$ to have a finite discontinuity at $x = 0$ and extend the definition of the delta function by writing

$$\lim_{\Delta x \to 0}\int_{-\Delta x}^{\Delta x} \Psi(x,y)\delta(x)dx = \frac{\Psi(0_+,y) + \Psi(0_-,y)}{2}. \tag{10}$$

After applying Eq. (10) in Eq. (9), we arrive to the boundary condition:

$$0 = -\imath\hbar v_F\sigma_x[\Psi(0_+,y) - \Psi(0_-,y)] + \frac{J}{2}\hat{\mathbf{S}}_e\cdot\hat{\mathbf{S}}_i[\Psi(0_+,y) - \Psi(0_-,y)]. \quad (11)$$

Assuming that we know the initial spinor state of the electron and quantum dot, we can solve the 12-variable equation system with Eq. (11). Now we focus on the probability amplitude of the scattered wave function if spin flip takes place (t_s) and if it does not (t_n):

$$t_n = \frac{64v_F^2\hbar^2 - 3J^2}{64v_F^2\hbar^2 - 16iv_F\hbar J + 3J^2} + O(\theta^2) \quad (12)$$

and

$$t_s = \frac{32iv_F\hbar J}{64v_F^2\hbar^2 - 16iv_F\hbar J + 3J^2} + O(\theta^2). \quad (13)$$

Notice that the Klein tunneling ($|t_n|^2 + |t_s|^2 = 1$) is present independently of the value of J when $\theta = 0$. The dependence of t_n and t_s on the incident angle θ reveals the resilience of the transmitted wave function in a region near to $\theta = 0$, where resonances are avoided. In the next section we will show how this is also the case for any other potential shape.

III. VALIDITY OF DELTA POTENTIAL APPROXIMATION

In order to prove the validity of the delta potential approximation, in this section we analyze the case in which the interaction potential has a square shape; any other potential shape can be built from square potentials with an infinitesimal length. The situation is depicted by the Hamiltonian:

$$\hat{H} = -i\hbar v_F\sigma\cdot\nabla + V\hat{\mathbf{S}}_e\cdot\hat{\mathbf{S}}_i\Theta\left(x - \frac{\Delta x}{2}\right)\Theta\left(x + \frac{\Delta x}{2}\right), \quad (14)$$

where $\Theta(x)$ is the Heaviside function and V and Δx are the constant height and the length of the barrier, respectively. To obtain the spinor-dependent transmittivity of the system, we express the ballistic electron-QD spinor in a singlet-triplet (ψ_-, ψ_+) basis. In these subspaces the dynamics are decoupled and the potential in Hamiltonian Eq. (14) can be considered as a spinless potential. The wave function describes the QD and the incident and reflected electron as

$$\Psi_{sq} = \begin{pmatrix}1\\ se^{i\theta}\end{pmatrix}\otimes(a\psi_+ + b\psi_-)e^{i(k_x x + k_y y)} + \begin{pmatrix}1\\ -se^{-i\theta}\end{pmatrix}\otimes(c\psi_+ + d\psi_-)re^{i(-k_x x + k_y y)}, \quad (15)$$

for $x \leqslant -\Delta x/2$, with $\epsilon_b = \hbar v_F\sqrt{k_x^2 + k_y^2}$ and $\theta = \tan^{-1}(k_y/k_x)$. In the region $-\Delta x/2 < x < \Delta x/2$, the wave function has a similar form:

$$\Psi_{sq} = \begin{pmatrix}1\\ se^{i\alpha}\end{pmatrix}\otimes(f\psi_+ + g\psi_-)e^{i(q_x x + k_y y)} + \begin{pmatrix}1\\ -se^{-i\alpha}\end{pmatrix}\otimes(h\psi_+ + j\psi_-)re^{i(-q_x x + k_y y)}, \quad (16)$$

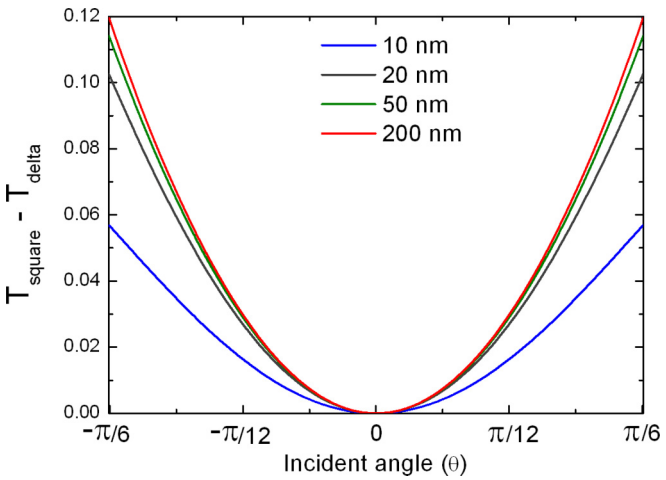

FIG. 2. (Color online) Difference between the square potential transmittivity (T_{square}) and the delta potential transmittivity ($T_\delta = |t_n|^2 + |t_s|^2$) as a function of small incident angles for different Δx values (10, 20, 50, and 200 nm). In all cases $\epsilon_b = 60$ meV, $J = 10$ eV Å, and $V = J/\Delta x$.

where $\epsilon_b - V = \hbar v_F\sqrt{q_x^2 + k_y^2}$ and $\alpha = \tan^{-1}(k_y/q_x)$, imposing continuity in k_y. Finally, the transmitted wave function is

$$\Psi_{sq} = \begin{pmatrix}1\\ se^{i\theta}\end{pmatrix}\otimes(\tau_+\psi_+ + \tau_-\psi_-)\,e^{i(k_x x + k_y y)}. \quad (17)$$

We evaluate the continuity of the wave function in the QD borders $x = -\Delta x/2$ and $\Delta x/2$, to obtain the probability amplitudes if spin flip takes place (τ_s) and if it does not (τ_n):

$$\tau_n = \frac{\tau_+ + \tau_-}{\sqrt{2}} = \frac{1}{\sqrt{2}}(e^{-\frac{iV}{4\hbar v_F}\Delta x} + e^{\frac{3iV}{4\hbar v_F}\Delta x}) + O(\theta^2) \quad (18)$$

and

$$\tau_s = \frac{\tau_+ - \tau_-}{\sqrt{2}} = \frac{1}{\sqrt{2}}(e^{-\frac{iV}{4\hbar v_F}\Delta x} - e^{\frac{3iV}{4\hbar v_F}\Delta x}) + O(\theta^2). \quad (19)$$

The total transmittivity $T_{\text{square}} = |\tau_n|^2 + |\tau_s|^2$ will remain approximately constant for small incident angles θ.To compare the effect of the potential shape, we plot in Fig. 2 the difference between the total transmittivity in the square potential (T_{square}) and delta potential ($T_\delta = |t_n|^2 + |t_s|^2$) cases, as a function of small incident angles and for different Δx values (10, 20, 50, and 200 nm). The square barrier height is set to be the average of the delta interaction as $V = J/\Delta x$, with $J = 10$ eV Å. The ballistic electron energy (ϵ_b) is 60 meV, which corresponds to a de Broglie wavelength of 70 nm, approximately. The difference is more pronounced as the incident angle becomes larger, which is due to the resonance present in nonfrontal injection. However, the difference is negligible for small angles ($< \pi/6$) even when the barrier length Δx is larger than the de Broglie wavelength. This allows us to validate the delta potential approach for a range of small incidence angles.

IV. A SCATTERING-BASED TWO-QUBIT GATE

We can now state the nontrivial conditions needed for a unitary quantum gate between a static and a scattered

qubit dependent on the founded probability amplitude transmission [5]. Usually, only the whole scattering process is unitary in the space and spin combined degree of freedom. If spin-flipped and no spin-flipped states of the mobile spin have different probabilities for transmission, then, by measuring the transmission, some information about the spin state can be acquired. This transformation is then clearly not unitary in the spin degree of freedom. The general transformation acting on the spin-density matrix ρ of the two qubits on transmission of the mobile spin is

$$\rho' = \frac{\mathbf{T}\rho\mathbf{T}^\dagger}{\mathrm{Tr}\,[\mathbf{T}\rho\mathbf{T}^\dagger]}, \tag{20}$$

where $\mathbf{T}$ is the probability amplitude matrix acting in a nonlinear way on ρ. The condition needed to assure unitarity and linearity of $\mathbf{T}$ is $|t_n + t_s| = |t_n t_s|$, with t_s and t_n the probability amplitudes defined in Sec. II. This is the condition to implement an electron-scattering quantum gate [5]. Not only it is very intricate to satisfy the gate condition for particles with Schrodinger dispersion, but the total transmission $|t_n|^2 + |t_s|^2$ in such cases is significantly lower than unity for useful two-qubit gates, making the gates nondeterministic.

It is straightforward to see in Eqs. (12) and (13) that the gate condition ($|t_n + t_s| = |t_n - t_s|$) is fulfilled independently of J in frontal scattering ($\theta = 0$), and the implemented gates will be deterministic. The cause of this behavior can be seen clearly if we express the system spinor in terms of the singlet-triplets basis ($\{\psi_-, |\uparrow\uparrow\rangle, \psi_+, |\downarrow\downarrow\rangle\}$), which are eigenfunctions of the Heisenberg operator; then the dynamics of the singlet and triplet subspaces are decoupled. In each of these subspaces, the Heisenberg interaction term of Eq. (3) reduces to a spinless potential barrier (similarly to what was done in the previous section) [5,28] so the effective Hamiltonian describes a particle scattering from two spin-independent potentials as

$$\hat{H}_S = -i\hbar v_F \sigma \cdot \nabla + V_S\,\delta(x), \tag{21}$$

where

$$V_S = \frac{J}{2}[S(S+1) - 3/2] \tag{22}$$

is an effective potential and S is the quantum number associated with $\hat{\mathbf{S}}^2$ and $S=0$ ($S=1$) in the case of the singlet (triplet). The ballistic electron, as a massless pseudo-Dirac fermion, can be perfectly transmitted through these potentials due to the Klein tunneling [15,18,22,23], and we expect that $|t_n + t_s| = |t_n - t_s|$ for any value of J.

In Eqs. (12) and (13) we can see that the angular dependence of the probability amplitudes in frontal insertion is resilient to small angular changes. Also, in frontal scattering the Klein tunneling is *independent of* k, and thereby it is present when the ballistic electron is in *an arbitrary wave packet*. In Fig. 3(a) we show the evolution of the probabilities of detecting a transmitted electron, or the success probability of the gate, $|t_n|^2 + |t_s|^2$ as a function of the incident angle θ and the coupling factor J. Notice that the gate success probability changes by only approximately 5% when θ changes from 0 to $\pm\pi/16$ and remains almost constant as J evolves.

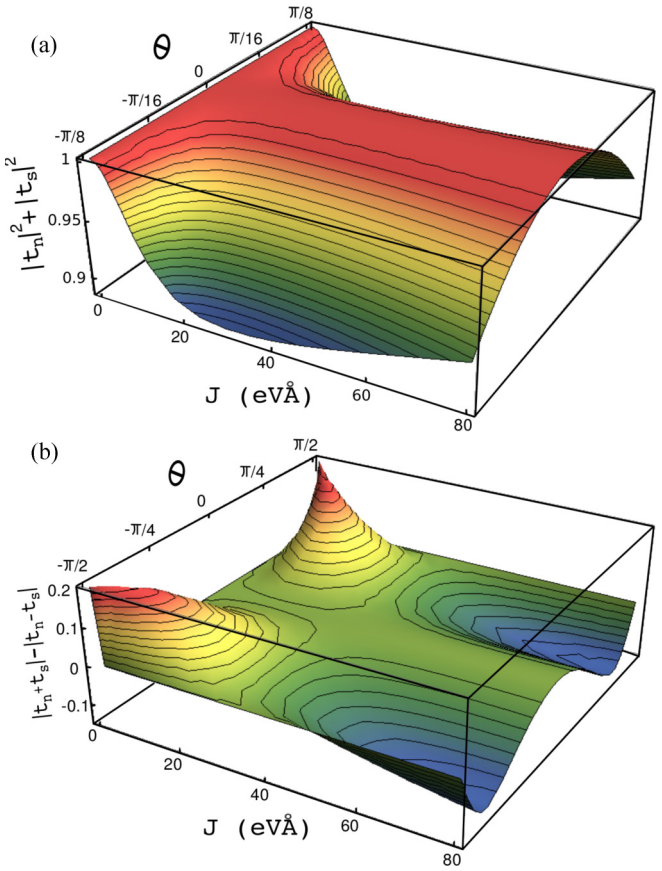

FIG. 3. (Color online) Evolution (a) of the gate probability of success ($|t_n|^2 + |t_s|^2$) and (b) of the gate condition $|t_n + t_s| - |t_n - t_s|$ as a function of the electron incident angle (θ) and the coupling factor (J).

We show $|t_n + t_s| - |t_n - t_s|$ as a function of variations in θ and J in Fig. 3(b); whenever $|t_n + t_s| - |t_n - t_s| = 0$, the gate condition is fulfilled [5]. Notice that this is satisfied in $J = 8\sqrt{1/3}\hbar v_F \approx 30$ eV Å, independently of the angle of incidence. The gates implemented here will be of SWAP type, which interchange the state of the two qubits. However, unless $\theta = 0$, there will be backscattering (gates will be nondeterministic). The implementation of this kind of gate can be useful to initialize and to read out the QD spin state, injecting a polarized ballistic electron, the final state of which can be measured directly.

In Fig. 4 we show the transmittivity or probability of a no-spin flip ($|t_n|^2$) and a spin flip ($|t_s|^2$) taking place after a frontal scattering, as a function of J. Notice that $|t_n|^2 = |t_s|^2$ for $J = 8\hbar v_F\sqrt{11 - 4\sqrt{7}}/3 \approx 11.2$ eV Å. At this point we expect to implement a $\sqrt{\mathrm{SWAP}}$ gate, generating maximum entanglement between the electron and QD spins.

The order of magnitude of J values we require is achievable. For example, for a $w = 30$-nm nanoribbon, a QD of $\Delta x = 21$ nm, an angle of $\theta \approx 22$ deg (a probability of success of 90% is obtained for 20 deg), and $\epsilon_b = 60$ meV, we obtain $t = 32$ meV, $U = 52$ meV, and thereby $J \approx 16.5$ eV Å. Although we have $U \sim 1.63t$, which would normally—for nonchiral particles—give a low but finite double occupancy (i.e., two mobile or two static electrons after scattering) probability of

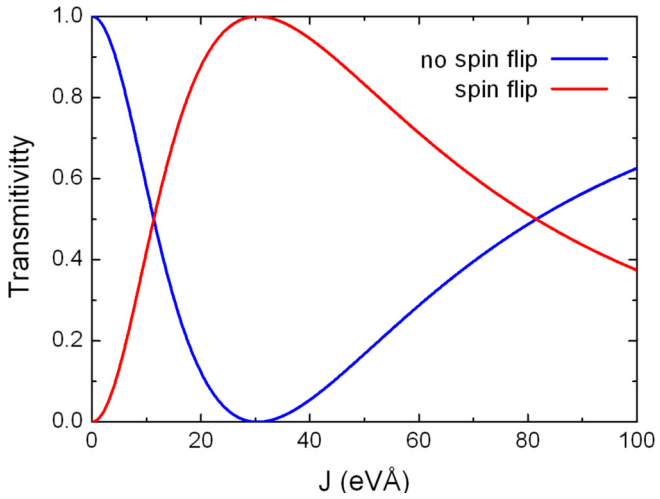

FIG. 4. (Color online) Transmittivity or probability of no spin flip ($|t_n|^2$ blue line) and a spin flip ($|t_s|^2$ reed line) after a frontal scattering, as a function of the coupling factor J.

about 27 %, here such processes should be suppressed by the conservation of pseudospin. Other parameter regimes may also be useful, as we show in the next section.

V. TWO QUANTUM DOT ENTANGLEMENT GENERATION

An application of this model is to use the ballistic electron spin as a mediator to relate two fixed and distant QDs. The separation between the two QDs can be in the micrometer range due to the graphene spin coherence length [29]. We can set the probability amplitudes of the electron scattering with the first (second) QD to be t_{n1} (t_{n2}) and t_{s1} (t_{s2}). If we inject a ballistic electron with a known spin state, for instance $|\uparrow\rangle_e$, the transformation is represented in the computational basis of the two QD spins ($|\uparrow\rangle_1|\uparrow\rangle_2$, $|\uparrow\rangle_1|\downarrow\rangle_2$, $|\downarrow\rangle_1|\uparrow\rangle_2$, $|\downarrow\rangle_1|\downarrow\rangle_2$) as

$$\mathbf{T}_2 = \begin{pmatrix} 1 & t_{s2} & t_{s1}t_{n2} & 0 \\ 0 & t_{n2} & t_{s1}t_{s2} & t_{s1} \\ 0 & 0 & t_{n1} & t_{n1}t_{s2} \\ 0 & 0 & 0 & t_{n1}t_{n2} \end{pmatrix}. \quad (23)$$

The triangular form of this matrix is due to the total transmission in the scattering events, so that the result on the second QD has no effect on the first one and no resonant behavior is expected. If we set the J factor of the second QD to be SWAP ($|t_{s2}| = 1$ and $|t_{n2}| = 0$), it is straightforward to see that after scattering with both QDs we obtain a superposition in the QD spin states of the form $\Psi_{12} = t_{s1}|\uparrow\rangle_1|\downarrow\rangle_2 + t_{s2}|\downarrow\rangle_1|\uparrow\rangle_2$. Thus, with this process we can control the level of entanglement generated. If we set the first QD J coefficient to implement a $\sqrt{\text{SWAP}}$ gate, or $|t_{s1}| = 1/\sqrt{2}$ and $|t_{n1}| = 1/\sqrt{2}$, we expect a total entangled final state between QD spins. It is not necessary to perform a postselection of any kind after the electron scattering.

Here let us point out that it is possible to choose different parameter regimes to obtain the values of J required above for the $\sqrt{\text{SWAP}}$ and SWAP. For example, for $W = 30$, $\epsilon_b = 65$ meV, and $\Delta x = 11$ nm, one obtains an angle of incidence of $\sim$21 deg (90% reflection occurs at 20 deg), $U = 66$ meV, $t = 25$ meV, and thereby $J \sim 4.1$ eV Å. For this value, the spin-flip probability on transmission is $\sim$0.1, and thereby the entangled state of impurity 1 and the ballistic spin that is generated is $\sim 0.95|\uparrow\rangle_e|\downarrow\rangle_1 + 0.31|\downarrow\rangle_e|\uparrow\rangle_1$. This is still an entangled state, and the fact that this is a result of a unitary operation makes the gate an entangling gate—which is still very useful for QIP, though not as readily useful as the maximally entangling $\sqrt{\text{SWAP}}$ gate. For example, taking the scenario of two static quantum dot based spins 1 and 2 mentioned above, but with the ballistic electron, initially in the $|\uparrow\rangle_e$ state, undergoing the same gate with both spins 1 and 2 (as opposed to the above case) in the parameter set of this paragraph, one can create the highly entangled state $0.69|\downarrow\rangle_1|\uparrow\rangle_2 + 0.73|\uparrow\rangle_1|\downarrow\rangle_2$ with a 0.18 success probability conditional on detecting the ballistic electron in the state $|\downarrow\rangle_e$ (say, by a spin filter).

VI. SUMMARY

In summary, in this work we have shown how the Klein tunneling, present in the graphene electrons scattering off a rectangular QD, is useful to implement quasideterministic (i.e., without backscattering) two-qubit quantum gates between the ballistic electron spin and the QD spin, and we have shown that this mechanism works for arbitrary electronic wave packets. The transversal confinement limits the incident angle in the scattering process, due to the quantization of the transverse wave vector k_y. This problem can be overcome tuning the ballistic electron energy to reach the frontal scattering ($\theta = 0$) angle asymptotically. We show that, when $J = 8\sqrt{1/3}\hbar v_F \approx$ 30 eV Å, a SWAP gate is obtained. In a frontal scattering, the Klein tunneling is present and we will always find quantum gates. The gates implemented in these conditions are quasideterministic, because the gate success depends on how approximately frontal the scattering is. However, we see that a change in the incident angle of $\pm\pi/16$ from the ideal frontal angle produces only small changes (of about 5%) in the gate success probability. It has also been shown how this model can be used to generate and control the entanglement between two fixed and distant QD spins, taking a ballistic electron spin as a mediator. Some of this work could be adaptable to a setting of carbon nanotubes, where a presence of backscattering is also absent.

ACKNOWLEDGMENTS

We thank Guido Burkard, Mark Buitelaar, John Jefferson, and Aires Ferreira for clarifying some aspects of the background literature. YO thanks the support from project IT-QuSim, as well as from Fundação para a Ciência e a Tecnologia (Portugal), namely through program POCTI/POCI/PTDC and projects PEst-OE/EGE/UI0491/2013, PEst-OE/EEI/LA0008/2013, and PTDC/EEA-TEL/103402/2008 QuantPrivTel, partially funded by FEDER (European Union), and from the EU FP7 projects LANDAUER (318287) and PAPETS (323901). SB is supported by the European Research Council. GCM acknowledges Consejo Nacional de Ciencia y Tecnología (Conacyt, México) for a postdoctoctoral grant. This research was partially funded by Conacyt, México, under Grant No. 83604.

[1] S. Hermelin *et al*., Nature (London) **477**, 435 (2011).
[2] R. P. G. McNell *et al*., Nature (London) **477**, 439 (2011).
[3] V. Miseikis, J. E. Cunningham, K. Saeed, R. ORorke, and A. G. Davies, Appl. Phys. Lett. **100**, 133105 (2012).
[4] T. Hiltunen and A. Harju, Phys. Rev. B **86**, 121301(R) (2012).
[5] G. Cordourier-Maruri, F. Ciccarello, Y. Omar, M. Zarcone, R. de Coss, and S. Bose, Phys. Rev. A **82**, 052313 (2010).
[6] F. Ciccarello, D. E. Browne, L. C. Kwek, H. Schomerus, M. Zarcone, and S. Bose, Phys. Rev. A **85**, 050305(R) (2012).
[7] A. T. Costa Jr., S. Bose, and Y. Omar, Phys. Rev. Lett. **96**, 230501 (2006).
[8] K. Yuasa and H. Nakazato, J. Phys. A **40**, 297 (2007).
[9] F. Ciccarello, M. Paternostro, M. S. Kim, and G. M. Palma, Phys. Rev. Lett. **100**, 150501 (2008).
[10] Y. Hida, H. Nakazato, K. Yuasa, and Y. Omar, Phys. Rev. A **80**, 012310 (2009).
[11] F. Ciccarello, M. Paternostro, G. M. Palma, and M. Zarcone, New J. Phys. **11**, 113053 (2009).
[12] F. Ciccarello, M. Paternostro, S. Bose, D. E. Browne, G. M. Palma, and M. Zarcone, Phys. Rev. A **82**, 030302(R) (2010).
[13] C. T. White and T. N. Todorov, Nature (London) **393**, 240 (1998).
[14] L. Balents and R. Egger, Phys. Rev. Lett. **85**, 3464 (2000).
[15] B. Trauzettel, D. V. Bulaev, D. Loss, and G. Burkard, Nature Phys. **3**, 192 (2007).
[16] M. Droth and G. Burkard, Phys. Rev. B **87**, 205432 (2013).
[17] K. S. Novoselov *et al*., Nature (London) **438**, 197 (2005).
[18] A. H. Castro Neto, F. Guinea, N. M. R. Peres, K. S. Novoselov, and A. K. Geim, Rev. Mod. Phys. **81**, 109 (2009).
[19] Y. Zhang *et al*., Appl. Phys. Lett. **86**, 073104 (2005).
[20] P. G. Silvestrov and K. B. Efetov, Phys. Rev. Lett. **98**, 016802 (2007).
[21] C. R. Dean *et al*., Nature Nanotechnology **5**, 722 (2010).
[22] M. I. Katsnelson, K. S. Novoselov, and A. K. Geim, Nature Phys. **2**, 620 (2006).
[23] A. F. Young and P. Kim, Nature Phys. **5**, 222 (2009).
[24] L. Brey and H. A. Fertig, Phys. Rev. B **73**, 235411 (2006).
[25] J. Tworzydlo, B. Trauzettel, M. Titov, A. Rycerz, and C. W. J. Beenakker, Phys. Rev. Lett. **96**, 246802 (2006).
[26] W.-K. Tse, E. H. Hwang and S. Das Sarma, Appl. Phys. Lett. **93**, 023128 (2008).
[27] D. Gunlycke, J. H. Jefferson, T. Rejec, A. Ramsak, D. G. Pettifor, and G. A. D. Briggs, J. Phys.: Condens. Matter **18**, S851 (2006).
[28] O. L. T. de Menezes and J. S. Helman, Am. J. Phys. **53**, 1100 (1985).
[29] A. R. Rocha, T. B. Martins, A. Fazzio and A. J. R. da Silva, Nanotechnology **21**, 345202 (2010).